A novel mixed-integer linear programming formulation of vanadium redox flow battery for energy management system applications considering dynamic nonlinearities

Hao Wang[a,*], S. Ali Pourmousavi[a], Wen L. Soong[a], Xinan Zhang[b]

[a] *School of Electrical & Mechanical Engineering, The University of Adelaide, Australia*
[b] *School of Engineering, The University of Western Australia, Australia*

Abstract

Accurate battery storage system modelling considering its nonlinear operational dynamics is crucial for achieving more economic benefits and higher flexibility. In this paper, a novel mixed-integer linear programming (MILP) formulation of vanadium redox flow batteries (VRFBs) is presented considering the dynamic nonlinear performance of charge losses and voltaic losses, as well as the actual battery management scheme. This research utilises a newly introduced multi-physics VRFB model, which incorporates all ion crossover and electrolyte transfer mechanisms to validate the model's effectiveness in precisely estimating the remaining energy. Rigorous simulation studies are conducted to validate the proposed model deployed in a residential energy management system (EMS) using 5-minute resolution data from residential consumers in Australia. The results show that the proposed MILP model achieves highly accurate remaining energy and economic benefit estimations, with power mismatch errors of less than 1%. Most importantly, the simulation results demonstrate that the proposed model results in up to 57.1% increase in economic benefits and 8.5% improvement in round-trip efficiency compared to traditional models that are widely used to estimate remaining energy.

Keywords: Remaining energy estimation, vanadium redox flow battery, optimal energy dispatch, energy management system, battery modelling

*Corresponding Author
Email address: hao.wang05@adelaide.edu.au

Nomenclature

α_{ch},β_{ch},γ_{ch}	Ideal charge power coefficients
α_{dch},β_{dch},γ_{dch}	Ideal discharge power coefficients
η_{ch}^{volt}, η_{dch}^{volt}	Charge/ discharge voltaic efficiency [%]
η_c	Coulombic efficiency [%]
η_{inv}	Inverter efficiency [%]
η_{rt}	Round-trip efficiency [%]
κ_φ	Membrane electro-kinetic permeability [m^2]
κ_e	Electrode hydraulic permeability [m^2]
κ_m	Membrane hydraulic permeability [m^2]
λ_{im}, λ_{ex}	Imported/exported cost from/to utility grid [A$/kWh]
λ_{KC}	Kozeny-Carman constant
μ_w	Mean viscosity of electrolyte [Pa $\cdot$ s]
ϕ_{ch}, τ_{ch}	Charge power regulation coefficients
ϕ_{dch}, τ_{dch}	Discharge power regulation coefficients
ϕ_{diff}^m	Effective diffusion potential [V]
ϕ_{neg}^m, ϕ_{pos}^m	Ionic potential at negative/positive sides [V]
ρ	Electrolyte density [kg m^{-3}]
ε	Electrode porosity
$\vec{v}_m$	Electrolyte velocity across membrane [m s^{-1}]
A_e	Cross-sectional area of porous electrode [m^2]
A_m	Membrane surface area [m^2]
A_t	Tank surface area [m^2]
c_i^s	Concentration of V^{i+} in the stack [mol L^{-1}]
c_i^t	Concentration of V^{i+} in tanks [mol L^{-1}]
c_f	Fixed acid concentration [mol L^{-1}]
C_{ideal}	Ideal capacity [Ah]

C_n	Nominal capacity [Ah]
C_p	Specific heat capacity of electrolyte [J g^{-1} K^{-1}]
c_{total}	Total concentration of V^{i+} [mol L^{-1}]
D	Thickness of the membrane [m]
d_f	Fibre diameter of the electrode [m]
$E^{0'}$	Formal potential [V]
E^{OCV}	Open-circuit voltage [V]
E_{ideal}	Ideal energy [kWh]
E_n	Nominal energy [kWh]
F	Faraday's constant [C mol^{-1}]
H_e	Height of the electrode [m]
I	Current [A]
I_{ch}, I_{dch}	Charge/ discharge current to/from battery [A]
k	Capacity loss rate [% s^{-1}]
k_{H^+}	Diffusion coefficient of H^+ [m^2 s^{-1}]
k_i	Diffusion coefficient of V^{i+} [m^2 s^{-1}]
L_e	Length of the electrode [m]
N	Number of cells in the stack
n_i^{con}	Convection fluxes of V^{i+} [mol m^{-2} s^{-1}]
n_i^{cross}	Overall crossover fluxes of V^{i+} [mol m^{-2} s^{-1}]
n_i^{diff}	Diffusion fluxes of V^{i+} [mol m^{-2} s^{-1}]
n_i^{mig}	Electro-migration fluxes of V^{i+} [mol m^{-2} s^{-1}]
P_{aux}	Power consumption of battery's auxiliary system [kW]
P_{ch}, P_{dch}	Charge/ discharge power to/from battery [kW]
P_{ch}^{ideal}, P_{dch}^{ideal}	Ideal charge/ discharge power to/from battery [kW]
P_{ch}^{max}, P_{ch}^{min}	Maximum/minimum charge power to battery [kW]
P_{dch}^{max}, P_{dch}^{min}	Maximum/minimum discharge power from battery [kW]
P_{im}, P_{ex}	Imported/exported power from/to utility grid [kW]

P_{load}	Load power [kW]
P_{re}	Renewable energy generation power [kW]
P_{self}	Self discharge power [W]
Q_c	Electrolyte flow rate in cell [L s^{-1}]
Q_s	Electrolyte flow rate of the system [L s^{-1}]
R	Gas constant [J $mol^{-1}K^{-1}$]
r'	Overall cell resistance [Ω]
R_s	Overall stack resistance [Ω]
SoC	State of charge [%]
SoE	State of energy [%]
T_p, T_n	Electrolyte temperature at positive/negative tank [K]
T_s	Electrolyte temperature in the stack [K]
T_{air}	Air temperature [K]
u_{ch}, u_{dch}	Battery charge/ discharge status
U_t	Heat transfer capability of tank [J K^{-1} s^{-1} m^{-2}]
V_p, V_n	Electrolyte volume of positive/negative tank [L]
V_s	Electrolyte volume of stack [L]
W_e	Width of the electrode [m]

1. Introduction

Battery technologies are recognised globally as a viable solution to address the issues associated with intermittent generation and non-dispatchable characteristics of renewable energy sources [1]. Among various battery technologies, vanadium redox flow batteries (VRFBs) are considered one of the most promising solutions for stationary energy storage applications with long-lasting performance and almost no degradation for 20 years [2]. The applications of VRFBs include industrial electrification, grid-scale energy storage, and residential energy storage solutions [3]. To this end, numerous large-scale VRFB projects have recently been implemented worldwide, usually located in conjunction with distributed energy resources (DERs), demonstrating a growing trend in VRFB deployment [1].

In the previously mentioned applications, VRFBs generally function within a broader system controlled by an energy management system (EMS) [4]. An EMS aims to optimise the operation of a hybrid system by anticipating its future state. For effective operation, an EMS requires accurate component models, such as battery models, to predict their future states. Consequently, accurate battery energy estimation models are crucial for the efficient functioning of an EMS.

Most EMS solves an optimisation problem to determine the optimal operating points of the hybrid system. Therefore, complex battery models are undesirable because of their intractability and high computational requirements. For example, the use of equivalent circuit models (ECMs) [5, 6] and electrochemical models (EMs) [7, 8, 9] is proposed in some EMS-related studies. The main difference is that conventional EMSs based on ECMs or EMs with model predictive control (MPC) or other online controllers are generally designed to tackle short-horizon charge/discharge control and optimisation problems to ensure efficient battery operation. In contrast, MILP formulations are designed for medium- to long-horizon energy arbitrage and planning, determine optimal future operating states (e.g. charge/discharge, power off, standby), and scale well while accommodating time-varying electricity tariffs and dynamic load power consumption. For these reasons, most previous work with MILP formulations on long-horizon optimal schedules with EMS for BESS energy management applications using a simple state of energy (SoE) model, typically with constant efficiency, and fixed battery energy parameters for the remaining energy estimation, considering different power system applications [10, 11, 12]. The simple SoE modelling approach does not take into account the internal chemical dynamics of battery systems, leading to an inaccurate estimation of the remaining energy inside the battery. Levin et al. identified accurate remaining energy estimation as the most important factor in securing dispatchable energy, demand-side flexibility and economic benefits, and capital revenue for investors and end users in battery projects [13]. Recently, the work by Wang et al. [3] revealed the problem of using simplified remaining energy approaches in poor techno-economic assessment outcomes in battery energy storage projects. This results in a low economic return and unsatisfactory expectations from battery owners, investors, and customers. To resolve the issues mentioned above, the authors in [14] and [15] proposed new mixed-integer linear programming (MILP) formulations to improve the optimal energy dispatch performance for Li-ion batteries. The findings of these studies indicate that the use of enhanced battery models can decrease the operational expenses of the BESS system, increase economic returns, and improve the feasibility of the solutions obtained by EMS. Recent studies, such as [10, 16, 17, 18, 19], have explored the degradation, multi-physics, and thermal behaviour of Li-ion batteries, and introduced simplified models to enhance the optimisation problem solved by EMS for decision making. From the literature, it seems that there is a profound lack of work on the development of a validated and accurate VRFB model for the EMS application. Considering that the efficiency of VRFB systems' varies more significantly under different operating load/current conditions compared to other batteries, an accurate model is important to ensure their high performance [20]. The works of Turker et al. in [21] and Jafari et al. in [22] proposed two similar MILP formulations for VRFBs taking into account the battery voltaic efficiency. However, constant round-trip efficiency is used in these studies, which neglects loss variations inside the VRFB system that can produce inaccurate estimates of remaining energy and economic benefits. Later, Cremoncini et al. presented a new MILP formulation for VRFB systems in [23], which considers voltaic efficiency, power consumption of the auxiliary system, and degradation. However, the results of the proposed model are not rigorously validated using an actual VRFB system or high-resolution multi-physics model. As a result, its accuracy of remaining energy estimation, energy dispatchability, and economic benefits remain unclear. Moreover, the coulombic efficiency has not been considered as another crucial efficiency factor in this work, and the BMS operation has also been neglected, for example, the universal constant current-constant voltage (CC-CV) charging method and standby losses. More importantly, earlier research on VRFBs overlooked the internal dynamics crucial for developing an accurate model of VRFBs. These oversights demonstrate the limitations of developing an accurate model that accounts for the nonlinearities in the chemical dynamics of VRFBs. This issue significantly

affects researchers and operators in fully exploring the potential and merits of VRFB in various power system applications, while also substantially reducing its competitiveness in the energy storage market.

To address these limitations, a novel MILP formulation is proposed and validated for a 5kW/10kWh VRFB system that incorporates all operational dynamics. A novel state of charge (SoC)-based model is also proposed to accurately estimate the remaining energy inside the VRFB system. The performance of the proposed MILP formulation is validated using a state-of-the-art multi-physics model, which is developed based on various ordinary differential equations (ODEs) and nonlinear formulations to describe the thermal, ionic, electrical potential, and fluid dynamics of VRFB systems. In-depth analyses are performed to illustrate the benefits of using a detailed battery model to increase operational revenue, round-trip efficiency, and accurate estimation of economic benefits compared to the conventional model.

The rest of the paper is organised as follows: Section 2 briefly introduces the limitations of using the conventional remaining energy estimation model. The MILP formulation and a novel remaining energy estimation model are proposed in Section 3. Finally, simulation results and in-depth evaluations of the benefits of using this newly proposed model are given in Section 4. The paper is concluded in Section 5 and future work is outlined.

2. Limitations of the conventional remaining energy estimation model

As mentioned previously, applying a simple remaining energy estimation model for VRFBs could have adverse effects on the energy supply and result in lower economic revenues for BESS. One such model is the SoE equation that is used in a large number of BESS optimal energy dispatch studies to estimate the remaining energy inside the BESS for various optimisation processes. The SoE is formulated using the following equation, which has been used in other works such as [3, 24, 25, 26, 27]:

$$SoE(t) = SoE(t-1) + \eta_{rt}\frac{P_{ch}(t)\Delta t}{E_n} - \frac{P_{dch}(t)\Delta t}{E_n} \tag{1}$$

Another popular form in the literature, e.g., in [28, 29, 30, 31, 32, 33], used in this study for comparison, is as follows:

$$SoE(t) = SoE(t-1) + \eta_{ch}\frac{P_{ch}(t)\Delta t}{E_n} - \frac{P_{dch}(t)\Delta t}{\eta_{dch}\,E_n} \tag{2}$$

where η_{rt} is the round-trip efficiency of the battery, $P_{ch}(t)$ and $P_{dch}(t)$ are the charge and discharge power of the battery at time t, η_{ch} and η_{dch} are the nominal charge and discharge efficiency of the battery, and E_n is the nominal energy (or available energy) of the battery defined in the manufacturer's datasheet. Most of the literature represents the round-trip efficiency η_{rt} and E_n as fixed values derived from the battery datasheet.

According to [3], a major issue is the limited availability of performance metrics for battery operators to effectively manage and schedule operations. These metrics are typically assessed under ideal conditions, such as an ambient temperature of 25°C and uniform charge/discharge power or current. As such, the efficiency of the BESS is likely to be overestimated compared to the battery performance under real-world operational conditions. This significantly restricts users from gathering detailed data on the efficiency behaviour of the battery for their intended uses. Furthermore, in real-world applications, the efficiency of VRFB can be impacted by several factors, such as fluctuation in power, the energy consumption of auxiliary systems, and standby

losses. Consequently, employing these basic SoE models without adequately accounting for efficiency variations may lead to erroneous predictions of the remaining energy in the optimisation problem.

3. A MILP formulation of VRFB

This section presents an innovative MILP formulation for VRFB, grounded in its true electrochemical and mechanical principles, along with a BMS operational scheme. The MILP formulation is based on a rigorous validated model that considers all the ion and electrolyte crossover mechanisms and the thermal dynamics of a 5kW VRFB system with a comprehensive BMS design as reported by Wang et al. in [34].

3.1. Vanadium redox flow battery

The VRFB is normally designed for residential-scale or medium- to large-scale energy storage systems with highly stable and low degradation performance over 20-30 years [1]. VRFBa are composed of several parts, including mainly two electrolyte storage tanks, a battery stack, a piping system, and two pumps for electrolyte circulation, as illustrated in Fig. 1. Most of the volume of the electrolyte is stored in the two electrolyte tanks, where the piping system forms a complete electrolyte circulation throughout the VRFB system. During battery operation, two pumps are operating to supply the vanadium ions for the main reactions in the stack, which are listed as follows:

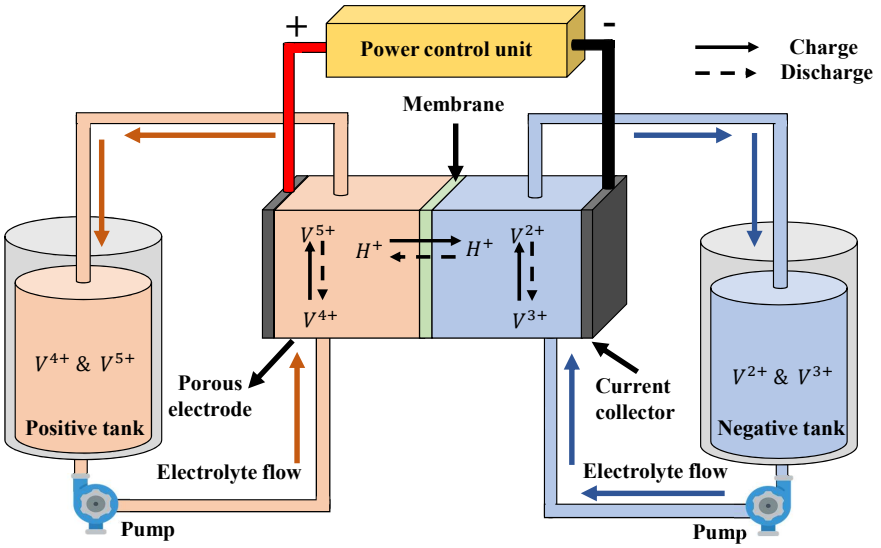

Figure 1: A schematic of a typical VRFB system showing its components and structure [35]

Negative half-cell reaction:

$$\mathrm{V}^{3+} + e^{-} \underset{\text{Discharge}}{\overset{\text{Charge}}{\rightleftharpoons}} \mathrm{V}^{2+} \tag{3}$$

Positive half-cell reaction:

$$VO^{2+} + H_2O \underset{\text{Discharge}}{\overset{\text{Charge}}{\rightleftharpoons}} VO_2^+ + 2H^+ + e^- \tag{4}$$

Overall cell reaction:

$$VO^{2+} + V^{3+} + H_2O \underset{\text{Discharge}}{\overset{\text{Charge}}{\rightleftharpoons}} VO_2^+ + V^{2+} + 2H^+ \tag{5}$$

3.2. VRFB remaining energy estimation formulation

The nature of the battery charge/discharge process is the movement of active species (charges) between the cathode and anode. In this case, the SoC is the only indicator for remaining energy estimation by BMS to prevent battery overcharging and discharging issues from occurring, which can be measured using the following equation:

$$SoC(t) = SoC(t-1) + \eta_c \frac{I_{ch}(t)\Delta t}{C_n} - \frac{I_{dch}(t)\Delta t}{C_n} \tag{6}$$

where η_c is the Coulombic efficiency and C_n is the nominal capacity in Ah measured in the battery discharge tests. $I_{ch}(t)$ and $I_{dch}(t)$ are the charging and discharging current at time t, respectively. However, this SoC estimation model is more accurate for Li-ion batteries with high and stable Coulombic efficiency (above 99% under different C-ratings [36]). In reality, VRFB systems exhibit a relatively low Coulombic efficiency (approximately 95% or lower) that fluctuates significantly with varying operational currents. Consequently, the SoC model in Eq. (6), which employs a constant Coulombic efficiency, proves to be inaccurate for VRFBs as it overlooks the dynamic self-discharge losses within the cells. Taking into account the self-discharge dynamics of VRFBs, in this work a new formulation for the estimation of SoC is proposed using capacity loss rates $k(t)$ in % per second instead of the Coulombic efficiency as given below:

$$SoC(t) = SoC(t-1) + \frac{I_{ch}(t)\Delta t}{C_{ideal}} - \frac{I_{dch}(t)\Delta t}{C_{ideal}} - k(t) \tag{7}$$

where C_{ideal} is the ideal capacity in Ah considering the total amount of active species in the battery system that remains almost constant for VRFB systems with almost no degradation. Compared with Eq. (6), this SoC formulation neglects the need to estimate the Coulombic efficiency for VRFB systems under different operational conditions. However, the SoC formulation in Eq. (7) is not ideal for optimisation problems since the current cannot be directly used as a decision variable in the optimal energy dispatch problem. This issue arises in the majority of VRFB optimal energy dispatch problems, where the decision variable is typically the VRFB power. In order to substitute the current-dependent variable in the SoC model, we introduce an innovative SoC formulation that uses VRFB power as the decision variable, which theoretically delivers equivalent performance, as demonstrated below.

$$SoC(t) = SoC(t-1) + \frac{P_{ch}^{ideal}(t)\Delta t}{E_{ideal}} - \frac{P_{dch}^{ideal}(t)\Delta t}{E_{ideal}} - k(t) \tag{8}$$

where E_{ideal} is the ideal energy in kWh of the VRFB without considering any losses and remains almost constant. $P_{ch}^{ideal}(t)$ and $P_{dch}^{ideal}(t)$ are the ideal charge and discharge power of the VRFB system without any loss at time t. The OCV is nearly identical at each capacity or SoC level regardless of the applied current, enabling precise SoC estimation using Eq. (8). The ideal capacity of the 5kW/10kWh VRFB system in Ah must be examined to determine the ideal energy of the

VRFB system in kWh without experiencing any charge losses. This contributes to accurately tracking the SoC of a VRFB system, which will be introduced in a later section. With the use of Faraday's law of electrolysis, the ideal capacity of this VRFB system is 282.5Ah considering the total amount of active vanadium ions. Furthermore, the ideal energy of the VRFB system in kWh can be obtained by integrating the OCV with the ideal capacity in the SoC range of 0% to 100%. The OCV versus ideal capacity is shown in Fig. 2. In this case, the ideal energy stored in the 5kW/10kWh VRFB system at 100% SoC is 14.6kWh as given below.

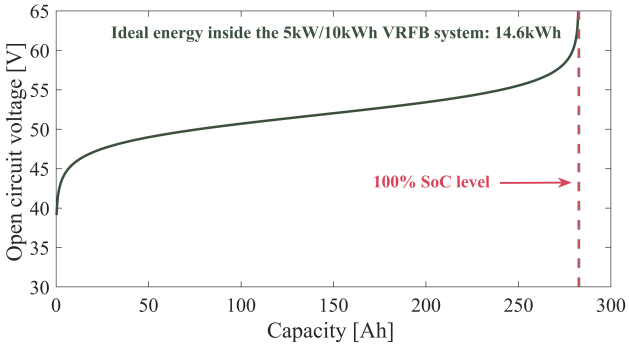

Figure 2: The OCV curve of the 5kW/10kWh VRFB system from zero capacity to 100% capacity

The $P_{ch}^{ideal}(t)$ and $P_{dch}^{ideal}(t)$ can be derived using OCV measurement from a reference cell in most commercial-scale VRFB-BMS designs. The equations to derive the ideal charging/discharging power are given below:

$$P_{ch}^{ideal}(t) = P_{ch}(t)\,\eta_{ch}^{volt}(t) = N\,I_{ch}(t)\,E^{OCV}(t) \tag{9}$$

$$P_{dch}^{ideal}(t) = \frac{P_{dch}(t)}{\eta_{dch}^{volt}(t)} = N\,I_{dch}(t)\,E^{OCV}(t) \tag{10}$$

where N, $\eta_{ch}^{volt}(t)$ and $\eta_{dch}^{volt}(t)$ are the number of cells in the stack and the voltaic efficiency of the battery during charge and discharge, respectively.

In the following section, we introduce the linearised modelling of the Coulombic loss rate and voltaic efficiency of the 5kW/10kWh VRFB system to achieve a highly accurate model to estimate the remaining energy in VRFBs using Eq. (8). It is important to point out that degradation modelling and thermal dynamics modelling are not essential factors in VRFB modelling for optimal dispatch problems. This is due to the fact that VRFB exhibits almost no signs of degradation over 10-20 years, as noted in [2]. Furthermore, most commercial VRFB exhibits highly stable thermal properties managed by BMS [37], which in this case its voltaic efficiency and Coulombic loss rate remaining relatively constant across a temperature range of 20-40°C.

3.3. Coulombic loss linearisation

The positioning of the membrane between the half cells facilitates the diffusion of vanadium ions, enabling their transfer across the half cells. This causes charge losses that reduce the SoC level in the VRFB system, commonly referred to as Coulombic loss. The losses inside the VRFB systems are caused by side reactions inside each of the cells. The movement of vanadium ions is driven by electro-migration, convection, and diffusion, which all account for the Coulombic

loss. However, for most commercial membrane designs with low electro-kinetic and hydraulic permeabilities, the electro-migration and convection have minor influences on the total crossover fluxes [35]. As a result, only modelling the Coulombic loss driven by diffusion is essential to estimate the SoC losses.

First, the Coulombic loss is modelled based on the simulation results of this 5kW/10kWh VRFB system. It is essential to note that Coulombic loss occurs not only during the operation of the VRFB system but also during the standby period when the electrolytes reside in the stack. The main distinction is that, during standby, the Coulombic loss leads to SoC losses in the stack because of the absence of electrolyte circulation. When the VRFB system is in operation, the electrolyte circulation will cause the electrolyte to be remixed, which decreases both the stack SoC and tank SoC levels. The Coulombic loss is mainly driven by concentration gradients in the form of diffusion [35]. As a result, their dynamics is almost unaffected by the operational current variations.

To model the Coulombic losses of this 5kW/10kWh VRFB system, model-based studies are carried out without applying current with electrolyte circulation alternately switched on and off. The results of the concentration losses of V^{2+} and V^{5+} are given in Fig. 3 (a). The V^{2+} and V^{5+} reflecting the remaining charge (SoC) inside the VRFB system as indicated in Eq. (A.16). It can be seen that, regardless of the electrolyte circulation condition, the charge losses exhibit a similar declining trend. However, it is important to note that V^{2+} experiences a higher decay rate due to its highest diffusivity on the Nafion 115 membrane [35]. Moreover, without electrolyte circulation, the concentration of V^{2+} in the stack has a significantly faster drop rate. This is because the electrolyte volume within the stack during battery operation represents a small portion of the total electrolyte volume in the entire VRFB system. To unify the Coulombic losses considering the total electrolyte volume of the system, the comparison of the overall SoC variations of the system by self-discharge with/without electrolyte circulation is depicted in Fig. 3 (b). In the upper figure, it can be observed that electrolyte circulation makes almost no change in charge losses. Furthermore, the capacity loss rates $k(t)$ (% per second) can be represented to estimate the Coulombic loss using a piecewise linearisation approach as a function of SoC, regardless of the operational mode. The results of using piecewise linear functions are presented in Fig. 3 (b), along with the SoC decay rate and the SoC range.

3.4. Ideal power modelling considering the voltaic losses

Another crucial factor in modelling the VRFB SoC, as illustrated in Eq. (8), is the accurate representation of the ideal battery power. As mentioned above, the energy stored in the VRFB system tends to vary with the operational conditions. Using the ideal power and ideal energy stored in the battery in Eq. (8) addresses the issue that the change of charge/ discharge power into/out of the VRFB system will influence its dispatchable energy (because the losses of the VRFB system are not considered). The ideal power results can be obtained using Eqs. (9) and (10). For commercial-scale VRFB systems, an OCV reference cell is typically integrated into the system to measure the OCV for SoC estimation. Therefore, OCV data can be collected by BMS to estimate the ideal power in real-world applications. Consequently, Figs. 4 (a) and (b) illustrate the 3D surfaces that represent the ideal power during the charge and discharge processes with respect to charge/ discharge power and the SoC. Two simple linear functions can model the ideal power during charging and discharging at each timestep t, as given below:

$$P_{ch}^{ideal}(t) = \alpha_{ch} + \beta_{ch} P_{ch}(t) + \gamma_{ch} SoC(t) \tag{11}$$

$$P_{dch}^{ideal}(t) = \alpha_{dch} + \beta_{dch} P_{dch}(t) + \gamma_{dch} SoC(t) \tag{12}$$

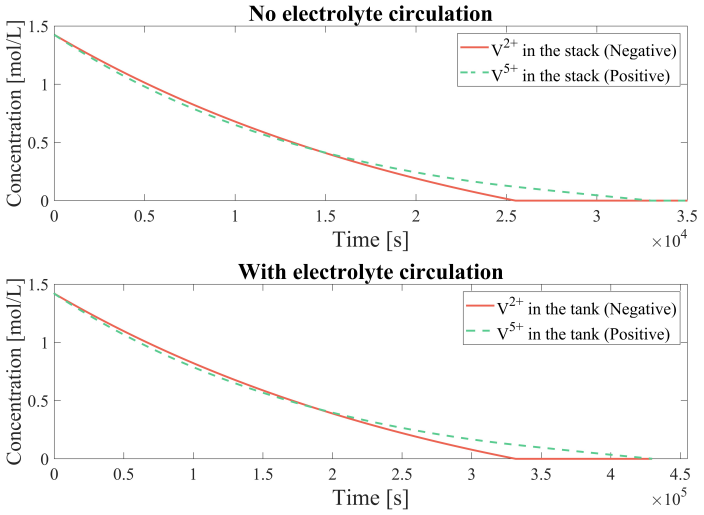

(a) The concentration losses of V^{2+} and V^{5+} from about 1.4 mol/L to 0 in the stack and tanks both with and without electrolyte circulation

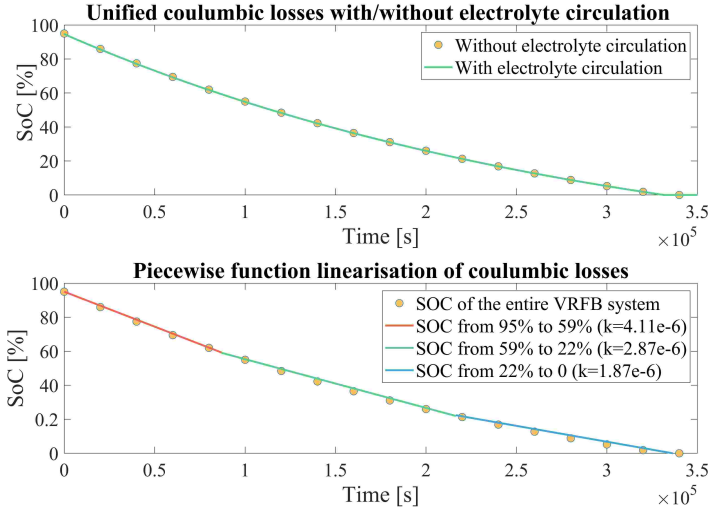

(b) The unified Coulombic losses in the SoC profile ranging from 95% to 0, both with and without electrolyte circulation, along with the piecewise linearisation results of the capacity decay rate k

Figure 3: The concentration and SoC losses in the stack and tank with/without electrolyte circulation and the linear piecewise approximation of the SoC decay.

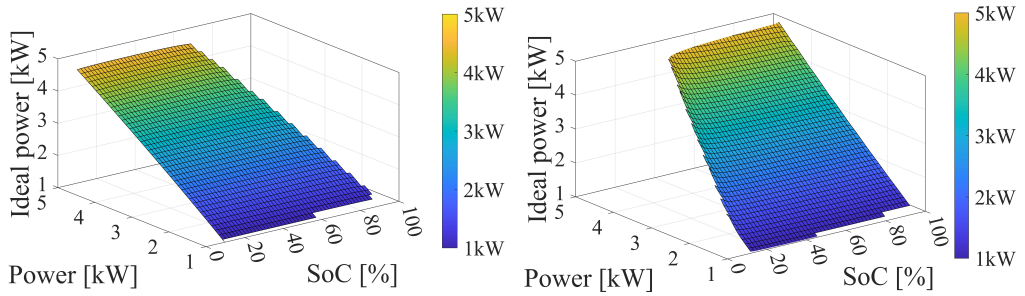

(a) The ideal charge power and operational charge power as a function of SoC

(b) The ideal discharge power and operational discharge power as a function of SoC

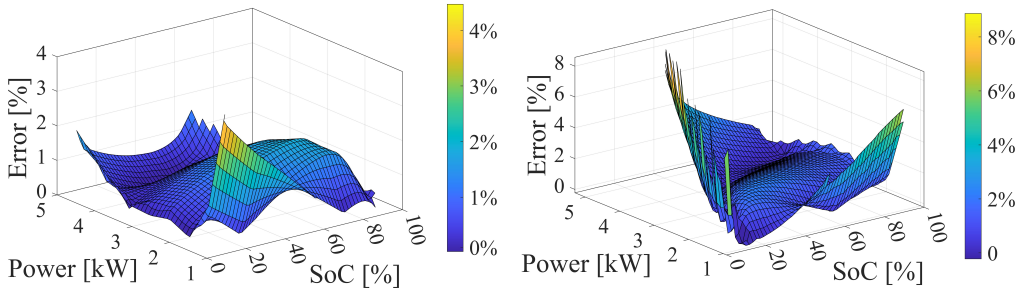

(c) The APE profiles of ideal power estimation vs. charge power and SoC (MAPE=1.02%, RMSE=11.00)

(d) The APE profiles of ideal power estimation vs. discharge power and SoC (MAPE=1.87%, RMSE=11.62)

Figure 4: The ideal power profiles during charging/discharging, the absolute percentage error (APE) profiles, mean absolute percentage error (MAPE) and root-mean-square error (RMSE) results using the linearised model of this 5kW/10kWh VRFB system

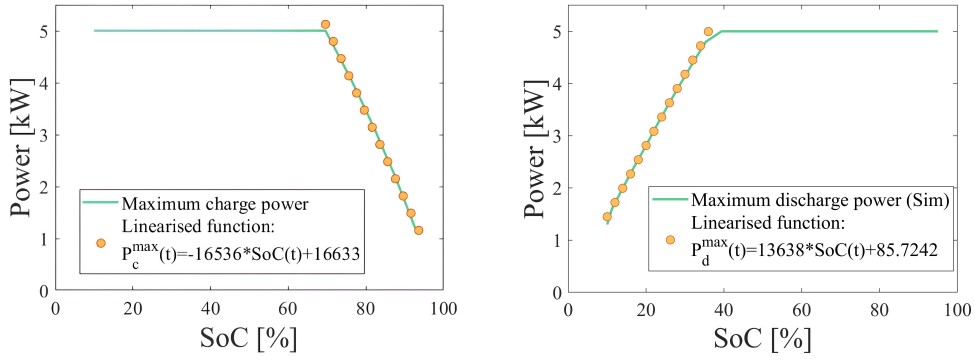

(a) The maximum charge power

(b) The maximum discharge power

Figure 5: The maximum charge and discharge power of the 5kW/10kWh VRFB system vs. SoC and linearised functions fitted for the SoC range

where α_{ch}, β_{ch} and γ_{ch} are the coefficients during charging, while α_{dch}, β_{dch} and γ_{dch} are for the battery model during discharging. $P_{ch}(t)$ and $P_{dch}(t)$ represent the power used to charge and discharge the VRFB system. The accuracy of these two linear functions is shown in Figs. 4 (c) and (d).

In addition, CC-CV is a universal charging method for commercial VRFB to prevent battery overcharging. VRFBs have relatively high concentration overpotential, which prevents the battery from being discharged at high power. To fully exploit the capacity, VRFB-BMS manages both the charge and discharge power. This means that both the charge and discharge power regulations must be considered in the VRFB model as a constraint to represent its true operational characteristics. The maximum charge and discharge power profiles versus SoC are given in Figs. 5 (a) and (b), respectively.

For any non-laboratory VRFB design, the power consumption from auxiliary components (such as pumps, BMS, and sensors) is significant and must be factored into the model. In this study, it is assumed that the auxiliary power supply for the battery system in charging mode is entirely derived from the connected power sources. However, during the discharging process, the auxiliary power is provided by the battery itself. As a result, the power regulation at each timestep can be modelled using the linear functions given below:

$$P_{ch}^{min} \leq P_{ch}(t) \leq \min(\tau_{ch} SoC(t) + \phi_{ch}, P_{ch}^{max}) \tag{13}$$

$$P_{dch}^{min} + P_{aux} \leq P_{dch}(t) \leq \min(\tau_{dch} SoC(t) + \phi_{dch}, P_{dch}^{max}) + P_{aux} \tag{14}$$

where P_{ch}^{min}, P_{dch}^{min}, P_{ch}^{max}, and P_{dch}^{max} represent the minimum and maximum charge and discharge power, respectively, managed by the BMS. Moreover, ϕ_{ch}, τ_{ch}, ϕ_{dch} and τ_{dch} are the power regulation coefficients for battery charging and discharging. P_{aux} is the total power consumption of the auxiliary components of the VRFB system.

3.5. Overall optimisation formulation

By integrating all the aforementioned constraints and taking into account the residential application of VRFBs for energy arbitrage to minimise the electricity cost from the utility grid considering renewable energy generation, the complete optimisation problem can be expressed as follows, where the decision variables are $\Theta = \{P_{ch}(t), P_{dch}(t), u_{ch}(t), u_{dch}(t), s(t)\}$:

$$\min_{\Theta} \quad \sum_{t\in\mathcal{H}} \Big[\lambda_{im}(t)\, P_{im}(t) - \lambda_{ex}(t) P_{ex}(t)\Big]\Delta t \tag{15a}$$

$$\text{s.t.} \quad P_{re}(t) + (P_{dch}(t) - P_{aux}) u_{dch}(t)\eta_{inv} - (P_{ch}(t) + P_{aux}) u_{ch}(t)/\eta_{inv} = P_{ex}(t) - P_{im}(t) + P_{load}(t) \quad \forall t \in \mathcal{H}' \tag{15b}$$

$$SoC(t) = SoC(t-1) + \frac{P_{ch}^{ideal}(t) u_{ch}(t) \Delta t}{E_{ideal}} - \frac{P_{dch}^{ideal}(t) u_{dch}(t) \Delta t}{E_{ideal}} - k(t) s(t) \quad \forall t \in \mathcal{H}, \tag{15c}$$

$$0 \leq u_{ch}(t) + u_{dch}(t) \leq 1 \quad \forall t \in \mathcal{H}, \tag{15d}$$

$$SoC(0) = SoC(t_f), \tag{15e}$$

$$SoC_{min} \leq SoC(t) \leq SoC_{max} \quad \forall t \in \mathcal{H}, \tag{15f}$$

$$s(t) = \begin{cases} 1 & \text{if } 0.1 < SoC(t) \leq 0.95 \\ 0 & \text{if } SoC(t) = 0.1 \end{cases}, \tag{15g}$$

$$k(t) = \begin{cases} 4.11 \times 10^{-6}\Delta t & \text{if } 0.10 \leq SoC(t) \leq 0.22 \\ 2.87 \times 10^{-6}\Delta t & \text{if } 0.22 \leq SoC(t) \leq 0.59 \\ 1.87 \times 10^{-6}\Delta t & \text{if } 0.59 \leq SoC(t) \leq 0.95 \end{cases}, \tag{15h}$$

$$P_{ch}^{ideal}(t) = \alpha_{ch} + \beta_{ch} P_{ch}(t) + \gamma_{ch} SoC(t) \quad \forall t \in \mathcal{H}, \tag{15i}$$

$$P_{dch}^{ideal}(t) = \alpha_{dch} + \beta_{dch} P_{dch}(t) + \gamma_{dch} SoC(t) \quad \forall t \in \mathcal{H}, \tag{15j}$$

$$P_{ch}^{min} \leq P_{ch}(t) \leq \min(\tau_{ch} SoC(t) + \phi_{ch}, P_{ch}^{max}) \quad \forall t \in \mathcal{H}, \tag{15k}$$

$$P_{dch}^{min} + P_{aux} \leq P_{dch}(t) \leq \min(\tau_{dch} SoC(t) + \phi_{dch}, P_{dch}^{max}) + P_{aux} \quad \forall t \in \mathcal{H} \tag{15l}$$

The overall objective function is given in Eq. (15a) in order to minimise the cost of electricity for users. In this equation, $\lambda_{im}(t)$ and $\lambda_{ex}(t)$ are the imported/exported prices of the energy from/to the utility grid. Furthermore, $P_{im}(t)$ and $P_{ex}(t)$ are the total imported/exported power from/to the utility grid for each consumer. The load power balance is given in Eq. (15b), where $P_{re}(t)$ and $P_{load}(t)$ are the power generation from renewable energy sources and the load power consumption, respectively. $\eta_{inv} = 0.95$ is the efficiency of the battery inverter, and $P_{aux} = 100$W is the auxiliary power consumption.

The proposed SoC estimation model is given in Eq. (15c). Eq. (15d) ensures that the VRFB system is not charged and discharged simultaneously. The initial charge must be equal to the remaining battery charge using Eq. (15e). The maximum and minimum SoC levels are enforced in Eq. (15f), that is, between 10% and 95% as noted in [35].

The battery operational state is given in Eqs. (15g) and (15h), where $s(t)$ is a binary decision variable that indicates the stop mode in which the VRFB system will be turned off, and $k(t)$ is used to model the self-discharge Coulombic losses of the 5kW/10kWh VRFB system using the piecewise linear model introduced in Section 3.3. Furthermore, Eqs. (15i)-(15l) calculate the ideal power during battery charging and discharging considering power management by BMS to obtain an accurate SoC estimation, as detailed in Section 3.4. Note that $\alpha_{ch} = 127.6$, $\beta_{ch} = 0.9$, $\gamma_{ch} = -52.9$ are the ideal charge power coefficients. In addition, $\alpha_{dch} = -79.9$, $\beta_{dch} = 1.14$, and $\gamma_{dch} = -133.9$ are ideal discharge power coefficients. These values are obtained using the piecewise linearisation approach based on the results of Figs. 4 (a) and (b). ϕ_{ch} and τ_{ch} are charge power regulation coefficients and ϕ_{dch} and τ_{dch} are discharge power regulation coefficients, whose values are given in Fig. 5.

4. Simulation study

In this section, the performance of the proposed MILP formulation is evaluated and compared with the conventional SoE estimation model, using real-world residential PV generation, load consumption and variable electricity tariffs [38]. A detailed multi-physics model of a VRFB introduced in Appendix A and a comprehensive VRFB-BMS design presented in [3] are used to represent the ground-truth operation of the 5kW/10kWh VRFB system over a 24-hour period for analysis and performance validation. The consumer aims to minimise electricity costs by using local generation, VRFB, and lower tariff periods to meet a specified daily electricity demand.

4.1. Simulation setup

We use real PV generation and load demand data from eight residential users in the Australian Capital Territory (ACT) [38]. The diagram illustrating this residential energy arbitrage application is shown in Fig. 6. Each residential user is assumed to be connected to the utility

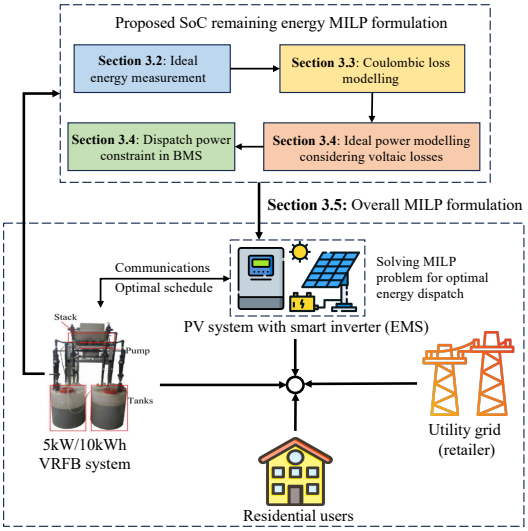

Figure 6: The schematic diagram of the residential energy arbitrage application of a VRFB system in this study with the proposed MILP formulation and optimisation in EMS

grid and owns a 5kW/10kWh VRFB system with a rooftop solar PV system and a smart inverter in an energy arbitrage scenario. The users are also assumed to be on the time-of-use tariff (ToU) and the solar feed-in tariff from Origin Energy obtained from December 2023 [39]. The smart inverter with EMS functionality takes into account the electricity tariff, ambient temperature and PV generation profiles to make the optimal energy dispatch decision with the use of the proposed MILP formulation for accurate remaining energy estimation and loss modelling introduced in previous sections. The optimisation problem is formulated using Eq. (15). To highlight the performance of the proposed model in accurate remaining energy estimation, a conventional and universal SoE-based remaining energy estimation model, presented in Eq. (1) which has been utilised in many related works such as [3, 24, 25, 26, 27] is used to replace the SoC-based remaining estimation models in Eq. (15) to formulate the following optimisation problem to find the decision variables Θ.

$$\min_{\Theta} \quad \sum_{t\in\mathcal{H}} \Big[\lambda_{im}(t)\, P_{im}(t) - \lambda_{ex}(t) P_{ex}(t)\Big]\Delta t \tag{16a}$$

$$\text{s.t.} \quad P_{re}(t) + (P_{dch}(t) - P_{aux}) u_{dch}(t)\, \eta_{inv} - (P_{ch}(t) + P_{aux}) \cdot u_{ch}(t)/\eta_{inv} = P_{ex}(t) - P_{im}(t) + P_{load}(t) \quad \forall t \in \mathcal{H}, \tag{16b}$$

$$SoE(t) = SoE(t-1) + \eta_{rt} \frac{(P_{ch}(t) + P_{aux}) u_{ch}(t) \Delta t}{E_n} - \frac{(P_{dch}(t) - P_{aux}) u_{dch}(t) \Delta t}{E_n} \quad \forall t \in \mathcal{H}, \tag{16c}$$

$$0 \le u_{ch}(t) + u_{dch}(t) \le 1 \quad \forall t \in \mathcal{H}, \tag{16d}$$

$$SoE(0) = SoE(t_f), \tag{16e}$$

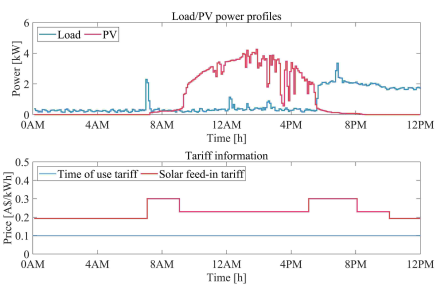

(a) The load and rooftop PV generation profiles of an anonymous user along with Origin Energy tariff information in Canberra, ACT

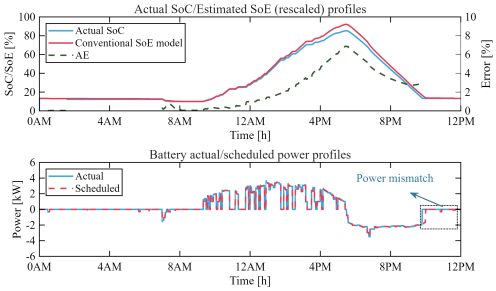

(b) The SoC and SoE profiles as well as actual and scheduled power profiles of the battery using conventional SoE estimation model with Eq. (1)

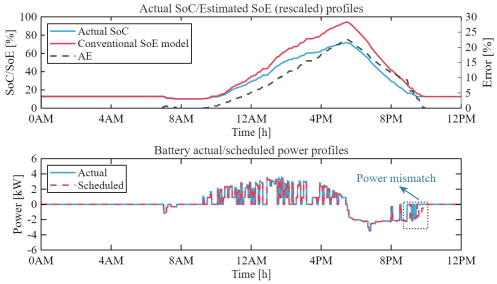

(c) The SoC and SoE profiles as well as actual and scheduled power profiles of the battery using conventional SoE estimation model with Eq. (2)

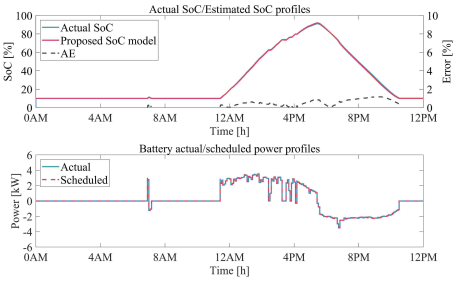

(d) The SoC and SoE profiles as well as actual and scheduled power profiles using the proposed SoC-based remaining energy estimation model

Figure 7: The SoC and SoE as well as actual and scheduled power profiles of the 5kW/10kWh VRFB system using different remaining energy estimation models for an anonymous user with a real tariff from Origin Energy, Australia

$$SoE_{min} \leq SoE(t) \leq SoE_{max} \quad \forall t \in \mathcal{H}, \tag{16f}$$

$$P_{ch}^{min} \leq P_{ch}(t) \leq \min(\tau_{ch} SoE(t) + \phi_{ch}, P_{ch}^{max}) \forall t \in \mathcal{H}, \tag{16g}$$

$$P_{dch}^{min} + P_{aux} \leq P_{dch}(t) \leq \min(\tau_{dch} SoE(t) + \phi_{dch}, P_{dch}^{max}) + P_{aux} \ \forall t \in \mathcal{H} \tag{16h}$$

The round-trip efficiency and nominal energy of the 5kW/10kWh VRFB system are 70% and 10kWh using $\eta_{rt} = \frac{\int_{t_0}^{t_f} (P_{dch}(t) - P_{aux}) dt}{\int_{t_0}^{t_f} (P_{ch}(t) + P_{aux}) dt}$ and $E_n = \int_{t_0}^{t_f} (P_{dch}(t) - P_{aux})\, dt$, respectively, based on the constant current discharge test and the CC-CV charge test results that consider the auxiliary system power consumption. $P_{ch}(t) + P_{aux}$ and $P_{dch}(t) - P_{aux}$ in Eq. 17c denote the total charge and discharge power for VRFB systems, taking into account auxiliary power consumption, crucial for operations such as pumping. Another SoE-based remaining estimation model considering the charge/discharge efficiency presented in Eq. (2) which has been utilised in many related works such as [28, 29, 30, 31, 32, 33], is used to devise an EMS, presented below:

$$\min_{\Theta} \quad \sum_{t \in \mathcal{H}} \Big[\lambda_{im}(t)\, P_{im}(t) - \lambda_{ex}(t) P_{ex}(t) \Big] \Delta t \tag{17a}$$

$$\text{s.t.} \quad \begin{aligned} &P_{re}(t) + (P_{dch}(t) - P_{aux})u_{dch}(t)\,\eta_{inv} - (P_{ch}(t) + P_{aux}) \cdot u_{ch}(t)/\eta_{inv} \\ &\qquad = P_{ex}(t) - P_{im}(t) + P_{load}(t) \quad \forall t \in \mathcal{H}, \end{aligned} \tag{17b}$$

$$\begin{aligned} SoE(t) = SoE(t-1) + \eta_{ch}\frac{(P_{ch}(t) + P_{aux})u_{ch}(t)\Delta t}{E_n} \\ -\frac{(P_{dch}(t) - P_{aux})u_{dch}(t)\Delta t}{\eta_{dch}\,E_n} \quad \forall t \in \mathcal{H}, \end{aligned} \tag{17c}$$

$$0 \le u_{ch}(t) + u_{dch}(t) \le 1 \quad \forall t \in \mathcal{H}, \tag{17d}$$

$$SoE(0) = SoE(t_f), \tag{17e}$$

$$SoE_{min} \le SoE(t) \le SoE_{max} \quad \forall t \in \mathcal{H}, \tag{17f}$$

$$P_{ch}^{min} \le P_{ch}(t) \le \min(\tau_{ch}SoE(t) + \phi_{ch}, P_{ch}^{max}) \forall t \in \mathcal{H}, \tag{17g}$$

$$P_{dch}^{min} + P_{aux} \le P_{dch}(t) \le \min(\tau_{dch}SoE(t) + \phi_{dch}, P_{dch}^{max}) + P_{aux}\ \forall t \in \mathcal{H} \tag{17h}$$

where under this definition, $\eta_{ch} \cdot \eta_{dch} = \eta_{rf}$ is set to consider energy conservation [40]. Since this VRFB system operates within the SoC range of 10% to 95%, the SoE profiles are adjusted from 0-100% to 10%-95% to represent the actual SoC levels in the figures. In this study, since capacity is restored using a hydraulic shunt rebalancing to address electrolyte volume disparities, these differences are excluded from the simulation [2].

4.2. Simulation results

4.2.1. Remaining energy estimation performance

Fig. 7 illustrates the simulation results obtained for an anonymous user as a demonstration. The load and PV power profiles and tariff information for a day are given in Fig. 7 (a). The results of the remaining energy estimation using the SoE and the proposed SoC models, as well as the actual and scheduled battery power, are given in Figs. 7 (b) and (c), respectively. It can be seen that the proposed estimation model achieves accurate results with a maximum absolute error of less than 2% (7% and 23% using the conventional SoE models in Eq. (1) and Eq. (2)) and a mean absolute error of 0.56% (3.2% and 5.8% using the conventional SoE estimation model in Eq. (1) and Eq. (2)).

Additional results are provided in Fig. 8, which illustrates the accuracy of the proposed SoC-based model to estimate the remaining energy. Absolute errors between the estimated remaining energy and the actual remaining energy for the conventional SoE model and the proposed SoC model of the eight users at different times of the day are given. As demonstrated by these two figures, the proposed SoC-based remaining energy model has considerably reduced the absolute error, achieving a mean absolute percentage error (MAPE) of 0.62% as opposed to 4.6% and 11.6% when using the SoE formulations in Eq. (1) and Eq. (2), respectively. This is achieved by considering the internal dynamic characteristics of VRFBs in the proposed MILP formulation using the SoC-based remaining energy estimation model.

4.2.2. Economic benefits and battery performance improvements

SoE models as presented in Eq. (1) and Eq. (2) or other basic remaining energy estimation approaches, which do not account for efficiency variations in VRFB technologies, can lead to negative operational outcomes. The key interest for users, operators, and investors lies in the economic benefits provided by VRFB operations. Hence, evaluating the effectiveness of the proposed approach in assessing the economic advantages of consumers is essential. Fig. 9 illustrates

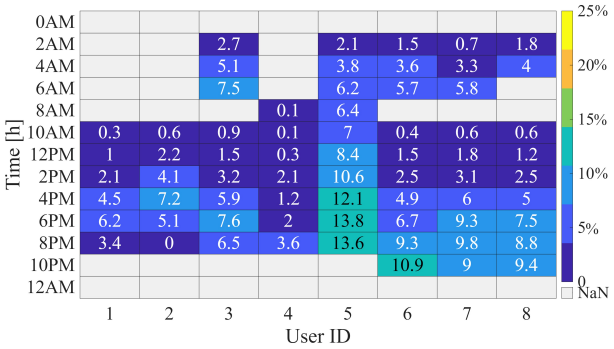

(a) SoE estimation using Eq. (1) with overall MILP formulation in Eq. (16)

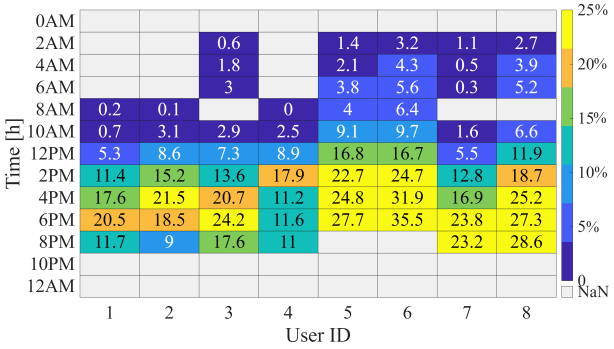

(b) SoE estimation using Eq. (2) with overall MILP formulation in Eq. (17)

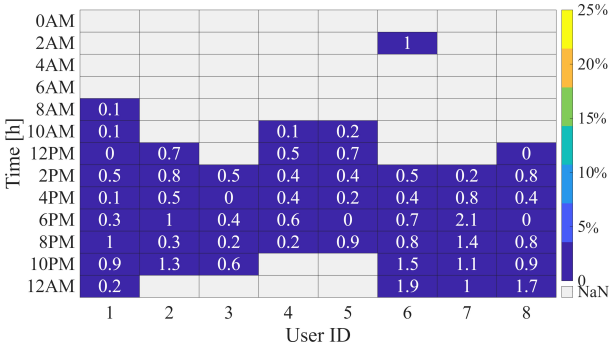

(c) Proposed linear SoC estimation

Figure 8: The absolute percentage errors (APE) in % between the estimated remaining energy and the actual remaining energy of 8 users over a day of simulation using three different remaining energy estimation models

the economic advantages and improved battery performance experienced by eight anonymous users when using the proposed SoC-based model, as opposed to the traditional SoE model. The advantages mentioned above can also be verified from the results in Table 1. The proposed

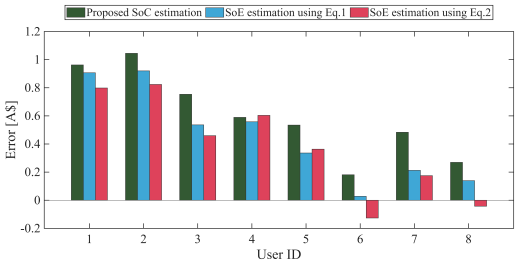

(a) The actual economic benefits profiles

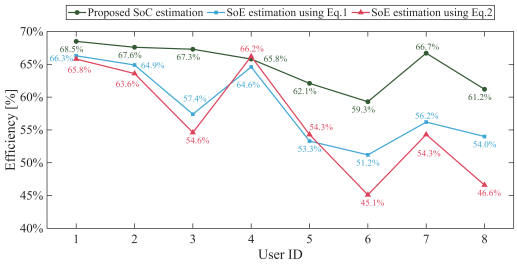

(b) The actual VRFB round-trip efficiency profiles

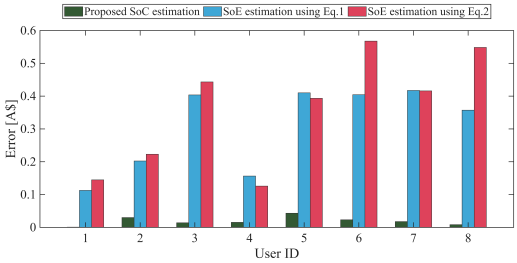

(c) The absolute errors between the estimated (at planning stage by EMS operation) and actual (at operating stage by multi-physics modelling

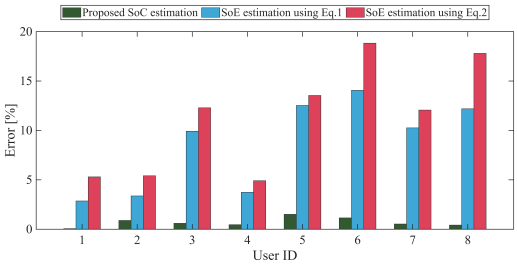

(d) The power mismatch profiles (absolute mean percentage error) between the scheduled power and actual power

Figure 9: The economic and operational performance of the 5kW/10kWh VRFB systems over a day of simulation for eight users by three remaining energy estimations

Table 1: Actual round-trip efficiency vs. estimated round-trip efficiency by the proposed MILP formulation

User ID	**10643**	**11887**	**12656**	**12662**
Actual round-trip efficiency [%]	68.47	67.57	67.25	65.80
Estimated round-trip efficiency (proposed MILP) [%]	68.47	68.66	67.87	66.33
Absolute error [%]	0.00	1.09	0.62	0.53
User ID	**13349**	**13592**	**13907**	**15866**
Actual round-trip efficiency [%]	62.08	59.33	66.65	61.19
Estimated round-trip efficiency (proposed MILP) [%]	63.98	60.75	67.29	61.69
Absolute error [%]	1.90	1.42	0.64	0.50

MILP formulation for SoC remaining estimation achieves an exceptionally low estimation error of 0.84% in predicting the actual round-trip efficiency, clearly demonstrating its capability to accurately model the dynamic losses during VRFB operation.Figure 9 (a) shows that the proposed SoC estimation method achieves higher economic benefits during one day of simulation with an overall 34.8% and 57.1% increase with respect to the SoE formulations in Eq. (1) and Eq. (2), respectively. The proposed SoC-based framework considers both the dynamic voltaic loss and the coulombic loss rate of 5kW/10kWh VRFB systems. This approach helps identify the optimal power scheduling for the VRFB by preventing the battery system from working under low-efficiency conditions.

The average round-trip efficiency profiles of the eight users over a day are given in Fig. 9 (b), which supports these results. It is evident that the proposed SoC estimation model generates a VRFB power profile that improves the round-trip efficiency of the VRFB system, thus boosting economic benefits. The average actual round-trip efficiency in one day of simulation using the proposed formulation reaches 64.8%, which is much higher than the two baseline cases using SoE formulations in Eq. (1) and Eq. (2), where it was only 58.5% and 56.3%, respectively. Further results in Figs. 9 (c) and (d) demonstrate that the proposed model achieves highly accurate economic benefit estimation and minimal power mismatch, compared to the traditional SoE estimation model. Due to the detailed loss modelling, the proposed method achieves more accurate remaining energy estimation, which consequently reduces the power mismatch errors from 8.6% and 11.3% using Eq. 1 and Eq. 2, respectively, to only 0.7%. The slight power mismatch leads to more precise decision-making, which in turn improves the accuracy of economic benefit estimates prior to operation. From the results, the proposed model reduces the MAPE of economic assessment from 67.8% and 93.7% using Eq. 1 and Eq. 2, respectively, to 3.1%. This provides investors with more reliable information and enables more accurate VRFB power scheduling for standby flexibility and uninterruptible power supply (UPS) services. Moreover, the proposed SoC-based model seamlessly integrates with optimisation formulations related to battery operation, which can be efficiently solved by various commercial and open source solvers.

5. Conclusion

Inaccurate models for the estimation of remaining energy in VRFB negatively affect the accurate assessment and achievement of their true economic value. To address this issue, this paper proposes a novel MILP formulation for VRFBs, incorporating a novel SoC-based remaining energy estimation model. Two main losses, the voltaic losses and charge losses, are modelled and linearised in the MILP formulation to accurately capture the system dynamics. Furthermore,

a practical battery management scheme for VRFB is considered as constraints in the proposed MILP formulation to achieve effectiveness in usable energy. Finally, a comprehensive MILP-based formulation is proposed to achieve effective and economic VRFB energy management considering residential applications. Comprehensive simulation studies are conducted using a newly proposed multi-physics model, which integrates all the mechanical and electrochemical dynamics of VRFB systems based on real data profiles from eight users in ACT, Australia. The simulation results demonstrate that the proposed MILP formulation provides a highly accurate estimate of the remaining energy compared to conventional SoE-based models. In particular, this led to an up to 57.1% increase in economic benefits and an up to 8.5% improvement in round-trip efficiency for daily battery operation. The findings emphasise the importance of developing an accurate battery model for commercial applications, and the proposed model could potentially be extended to other battery types.

Declaration of Generative AI and AI-assisted technologies in the writing process

During the preparation of this work, the authors used Grammarly/ChatGPT for grammar checking. After using these tools, the authors reviewed and edited the content as needed and take full responsibility for the content of the publication.

Acknowledgment

This project is supported by the Australian Government Research Training Program (RTP) through the University of Adelaide, and a supplementary scholarship is provided by the Micro-grid Battery Deployment project, which is funded by the Future Battery Industries Cooperative Research Centre (FBICRC) as part of the Commonwealth Cooperative Research Centre Program, Australia.

Appendix A: Multi-physics model formation of the 5kW/10kWh VRFB system

This Appendix presents the multi-physics model and parameters of the 5kW/10kWh VRFB system. For more details, refer to our earlier work in [34].

For vanadium ions in the cell:

$$\frac{dc_2^s}{dt} = \frac{Q_c\left(c_2^t - c_2^s\right) \pm \frac{I}{zF} - n_2^{cross}A_m - 2n_5^{cross}A_m - n_4^{cross}A_m}{L_e W_e H_e} \tag{A.1}$$

$$\frac{dc_3^s}{dt} = \frac{Q_c\left(c_3^t - c_3^s\right) \mp \frac{I}{zF} - n_3^{cross}A_m + 3n_5^{cross}A_m + 2n_4^{cross}A_m}{L_e W_e H_e} \tag{A.2}$$

$$\frac{dc_4^s}{dt} = \frac{Q_c\left(c_4^t - c_4^s\right) \mp \frac{I}{zF} - n_4^{cross}A_m + 3n_2^{cross}A_m + 2n_3^{cross}A_m}{L_e W_e H_e} \tag{A.3}$$

$$\frac{dc_5^s}{dt} = \frac{Q_c\left(c_5^t - c_5^s\right) \pm \frac{I}{zF} - n_5^{cross}A_m - 2n_2^{cross}A_m - n_3^{cross}A_m}{L_e W_e H_e} \tag{A.4}$$

It should be noted that the overall fluxes (n_i^{cross}) in Eqs. (A.1)-(A.4) include the diffusion fluxes (n_i^{diff}), convection fluxes (n_i^{con}) and electro-migration fluxes (n_i^{mig}), and can be computed

as follows:

$$n_i^{cross} = n_i^{diff} + n_i^{con} + n_i^{mig} = k_i \frac{c_i}{D} + \vec{v}_m c_i + \frac{z_i F}{RT} k_i c_i \nabla(\phi_{neg}^m - \phi_{pos}^m) \tag{A.5}$$

For the vanadium ions in the tanks, we have the following governing equations:

$$(V_n + N\,\Delta V_n)\frac{dc_2^t}{dt} = Q_s\,(c_2^s - c_2^t) \tag{A.6}$$

$$(V_n + N\,\Delta V_n)\frac{dc_3^t}{dt} = Q_s\,(c_3^s - c_3^t) \tag{A.7}$$

$$(V_p + N\,\Delta V_p)\frac{dc_4^t}{dt} = Q_s\,(c_4^s - c_4^t) \tag{A.8}$$

$$(V_p + N\,\Delta V_p)\frac{dc_5^t}{dt} = Q_s\left(c_5^s - c_5^t\right) \tag{A.9}$$

Note that in Eqs. (A.6)-(A.9), ΔV_p and ΔV_n are the rates of electrolyte transfer driven by osmotic pressure and ionic potential in the electrolyte. The electrolyte velocity across the membrane can be represented by the following equation.

$$\vec{v}_m = \frac{\kappa_m}{D}\frac{L_e}{2\kappa_e A_e}\left(Q_c - \frac{\mu^+}{\mu^-}Q_c\right) - \frac{\kappa_\varphi}{\mu_w}c_f F\left(\frac{I}{\sigma_m A_m} + \phi_{diff}^m\right) \tag{A.10}$$

Thus, the electrolyte volume transfer rate can be determined as follows:

$$\Delta V_n = -\Delta V_p = \vec{v}_m\, A_m \tag{A.11}$$

The open-circuit voltage (OCV) of a single cell, E^{OCV}, is:

$$E^{OCV} = E^{0\prime} + \frac{RT}{zF}\ln\left(\frac{c_2^s c_5^s}{c_3^s c_4^s}\right); E^{0\prime} = 1.40\ \text{V} \tag{A.12}$$

In this analysis, the formal potential $E^{0\prime}$ disregards the minor impact of enthalpy variation, as established by Xiong et al. [41] for the 5kW VRFB stack. The stack voltage is composed of OCV, ohmic overpotential and concentration overpotential of each cell, which can be derived using the following equations for charging and discharging, respectively [42]:

$$E_s = N\left[E^{0\prime} + \frac{RT}{zF}\ln\left(\frac{c_2^s c_5^s}{c_3^s c_4^s}\right) + Ir' - \frac{RT}{zF}\ln\left(1 - \frac{I}{k_m F L_e H_e c_3^s}\right) - \frac{RT}{zF}\ln\left(1 - \frac{I}{k_m F L_e H_e c_4^s}\right)\right] \tag{A.13}$$

$$E_s = N\left[E^{0\prime} + \frac{RT}{zF}\ln\left(\frac{c_2^s c_5^s}{c_3^s c_4^s}\right) - Ir' + \frac{RT}{zF}\ln\left(1 - \frac{I}{k_m F L_e H_e c_5^s}\right) + \frac{RT}{zF}\ln\left(1 - \frac{I}{k_m F L_e H_e c_2^s})\right)\right] \tag{A.14}$$

The k_m is the mass transfer coefficient in dm s^{-1}:

$$k_m = 1.6 \times 10^{-3}\left(\frac{Q_c}{10 L_e W_e}\right)^{0.4} \tag{A.15}$$

The SoC of the VRFB system is described using the following equation that accounts for the system imbalance:

$$SoC = \min\left(\frac{c_2^t}{c_2^t + c_3^t}, \frac{c_5^t}{c_4^t + c_5^t}\right) \tag{A.16}$$

The thermal model of this VRFB system is derived from the principles of the energy conservation law [37]. The electrolyte temperature within the stack is affected by self-discharge

reactions, changes in entropy, internal heat production, and heat exchange, as described by the following equation:

$$C_p \rho V_s \frac{dT_s}{dt} = Q_s C_p \rho \left(T_p - T_s\right) + Q_s C_p \rho \left(T_n - T_s\right) + I T_s \frac{dE}{dT} + P_{self} + I^2 R_s \tag{A.17}$$

The electrolyte temperature in positive/negative tanks is:

$$C_p \rho V_p \frac{dT_p}{dt} = Q_s C_p \rho \left(T_s - T_p\right) + U_t A_t \left(T_{air} - T_p\right) \tag{A.18}$$

$$C_p \rho V_n \frac{dT_n}{dt} = Q_s C_p \rho \left(T_s - T_n\right) + U_t A_t \left(T_{air} - T_n\right) \tag{A.19}$$

References

[1] Hao Wang, S Ali Pourmousavi, Wen L Soong, Xinan Zhang, and Nesimi Ertugrul. Battery and energy management system for vanadium redox flow battery: A critical review and recommendations. *Journal of Energy Storage*, 58:106384, 2023.

[2] Yifeng Li, David Kienbaum, Thomas Lüth, and Maria Skyllas-Kazacos. Long term performance evaluation of a commercial vanadium flow battery system. *Journal of Energy Storage*, 90:111790, 2024.

[3] Hao Wang, S Ali Pourmousavi, Wen L Soong, Xinan Zhang, and Rui Yuan. Accurate battery models matter: Improving battery performance assessment using a novel energy management architecture. *Journal of Power Sources*, 631:236216, 2025.

[4] Tiancheng Ouyang, Mingliang Zhang, Peijia Qin, and Xianlin Tan. Flow battery energy storage system for microgrid peak shaving based on predictive control algorithm. *Applied Energy*, 356:122448, 2024.

[5] Shunli Wang, Daniel-Ioan Stroe, Carlos Fernandez, Chunmei Yu, Chuanyun Zou, and Xiaoxia Li. A novel energy management strategy for the ternary lithium batteries based on the dynamic equivalent circuit modeling and differential kalman filtering under time-varying conditions. *Journal of Power Sources*, 450:227652, 2020.

[6] Hongwen He, Rui Xiong, Hongqiang Guo, and Shuchun Li. Comparison study on the battery models used for the energy management of batteries in electric vehicles. *Energy Conversion and Management*, 64:113–121, 2012.

[7] Luca De Pascali, Francesco Biral, and Simona Onori. Aging-aware optimal energy management control for a parallel hybrid vehicle based on electrochemical-degradation dynamics. *IEEE Transactions on Vehicular Technology*, 69(10):10868–10878, 2020.

[8] Yizhao Gao, Chong Zhu, Xi Zhang, and Bangjun Guo. Implementation and evaluation of a practical electrochemical-thermal model of lithium-ion batteries for ev battery management system. *Energy*, 221:119688, 2021.

[9] Weihan Li, Decheng Cao, Dominik Jöst, Florian Ringbeck, Matthias Kuipers, Fabian Frie, and Dirk Uwe Sauer. Parameter sensitivity analysis of electrochemical model-based battery management systems for lithium-ion batteries. *Applied Energy*, 269:115104, 2020.

[10] Mohammad Amini, Mehrdad Bagheri Sanjareh, Mohammad Hassan Nazari, GB Gharehpetian, and Seyed Hossein Hosseinian. A novel model for battery optimal sizing in microgrid planning considering battery capacity degradation process and thermal impact. *IEEE Transactions on Sustainable Energy*, 2024.

[11] Shahab Karrari, Nicole Ludwig, Giovanni De Carne, and Mathias Noe. Sizing of hybrid energy storage systems using recurring daily patterns. *IEEE Transactions on Smart Grid*, 13(4):3290–3300, 2022.

[12] He Hao, Di Wu, Jianming Lian, and Tao Yang. Optimal coordination of building loads and energy storage for power grid and end user services. *IEEE Transactions on Smart Grid*, 9(5):4335–4345, 2017.

[13] Todd Levin, John Bistline, Ramteen Sioshansi, Wesley J Cole, Jonghwan Kwon, Scott P Burger, George W Crabtree, Jesse D Jenkins, Rebecca O'Neil, Magnus Korpås, et al. Energy storage solutions to decarbonize electricity through enhanced capacity expansion modelling. *Nature Energy*, 8(11):1199–1208, 2023.

[14] Alvaro Jose Gonzalez-Castellanos, David Pozo, and Aldo Bischi. Non-ideal linear operation model for li-ion batteries. *IEEE Transactions on Power Systems*, 35(1):672–682, 2019.

[15] Kyriaki Antoniadou-Plytaria, David Steen, Ola Carlson, Mohammad Ali Fotouhi Ghazvini, et al. Market-based energy management model of a building microgrid considering battery degradation. *IEEE Transactions on Smart Grid*, 12(2):1794–1804, 2020.

[16] Chunyang Liu, Houzhen Ma, Hengxu Zhang, Xiaohan Shi, and Fang Shi. A MILP-based battery degradation model for economic scheduling of power system. *IEEE Transactions on Sustainable Energy*, 14(2):1000–1009, 2022.

[17] Yuanbo Chen, Kedi Zheng, Yuxuan Gu, Jianxiao Wang, and Qixin Chen. Optimal energy dispatch of grid-connected electric vehicle considering lithium battery electrochemical model. *IEEE Transactions on Smart Grid*, 2023.

[18] David Domínguez-Barbero, Javier García-González, Miguel Á Sanz-Bobi, and Aurelio García-Cerrada. Energy management of a microgrid considering nonlinear losses in batteries through deep reinforcement learning. *Applied Energy*, 368:123435, 2024.

[19] Arshad Nawaz, Jing Wu, Jun Ye, Yidi Dong, and Chengnian Long. Distributed mpc-based energy scheduling for islanded multi-microgrid considering battery degradation and cyclic life deterioration. *Applied Energy*, 329:120168, 2023.

[20] Abraham Alem Kebede, Theodoros Kalogiannis, Joeri Van Mierlo, and Maitane Berecibar. A comprehensive review of stationary energy storage devices for large scale renewable energy sources grid integration. *Renewable and sustainable energy reviews*, 159:112213, 2022.

[21] Burak Turker, Sebastian Arroyo Klein, Eva-Maria Hammer, Bettina Lenz, and Lidiya Komsiyska. Modeling a vanadium redox flow battery system for large scale applications. *Energy conversion and management*, 66:26–32, 2013.

[22] Mehdi Jafari, Kara Rodby, John Leonard Barton, Fikile Brushett, and Audun Botterud. Improved energy arbitrage optimization with detailed flow battery characterization. In *2019 IEEE Power & Energy Society General Meeting (PESGM)*, pages 1–5. IEEE, 2019.

[23] Diana Cremoncini, Guido Francesco Frate, Aldo Bischi, and Lorenzo Ferrari. Mixed integer linear program model for optimized scheduling of a vanadium redox flow battery with variable efficiencies, capacity fade, and electrolyte maintenance. *Journal of Energy Storage*, 59:106500, 2023.

[24] Yu Zheng, Junhua Zhao, Yue Song, Fengji Luo, Ke Meng, Jing Qiu, and David John Hill. Optimal operation of battery energy storage system considering distribution system uncertainty. *IEEE Transactions on Sustainable Energy*, 9(3):1051–1060, 2017.

[25] Lei Chen, Shunli Wang, Hong Jiang, and Carlos Fernandez. A multi-time-scale framework for state of energy and maximum available energy of lithium-ion battery under a wide operating temperature range. *Applied Energy*, 355:122225, 2024.

[26] David M Rosewater, David A Copp, Tu A Nguyen, Raymond H Byrne, and Surya Santoso. Battery energy storage models for optimal control. *IEEE Access*, 7:178357–178391, 2019.

[27] Majid Moradzadeh and Morad Mohamed Abdelmageed Abdelaziz. A new milp formulation for renewables and energy storage integration in fast charging stations. *IEEE Transactions on Transportation Electrification*, 6(1):181–198, 2020.

[28] Riccardo Nebuloni, Lorenzo Meraldi, Cristian Bovo, Valentin Ilea, Alberto Berizzi, Snigdh Sinha, Raviteja Bharadwaj Tamirisakandala, and Pietro Raboni. A hierarchical two-level milp optimization model for the management of grid-connected bess considering accurate physical model. *Applied Energy*, 334:120697, 2023.

[29] Paolo Marocco, Domenico Ferrero, Emanuele Martelli, Massimo Santarelli, and Andrea Lanzini. An milp approach for the optimal design of renewable battery-hydrogen energy systems for off-grid insular communities. *Energy Conversion and Management*, 245:114564, 2021.

[30] Yaling Wu, Zhongbing Liu, Jiangyang Liu, Hui Xiao, Ruimiao Liu, and Ling Zhang. Optimal battery capacity of grid-connected pv-battery systems considering battery degradation. *Renewable Energy*, 181:10–23, 2022.

[31] Jide Niu, Zhe Tian, Yakai Lu, and Hongfang Zhao. Flexible dispatch of a building energy system using building thermal storage and battery energy storage. *Applied Energy*, 243:274–287, 2019.

[32] Yinghua Jiang, Lixia Kang, and Yongzhong Liu. Optimal configuration of battery energy storage system with multiple types of batteries based on supply-demand characteristics. *Energy*, 206:118093, 2020.

[33] Xiong Wu, Wencheng Zhao, Xiuli Wang, and Haoyu Li. An milp-based planning model of a photovoltaic/diesel/battery stand-alone microgrid considering the reliability. *IEEE Transactions on Smart Grid*, 12(5):3809–3818, 2021.

[34] Hao Wang, S Ali Pourmousavi, Wen L Soong, Xinan Zhang, Aleksandar N Nikoloski, and Nesimi Ertugrul. A comprehensive and practical framework for advanced battery management system of vanadium redox flow batteries. *Journal of Energy Storage*, 123:116560, 2025.

[35] Hao Wang, S Ali Pourmousavi, Yifeng Li, Wen L. Soong, Xinan Zhang, and Bingyu Xiong. A new zero-dimensional dynamic model to study the capacity loss mechanism of vanadium redox flow batteries. *Journal of Power Sources*, 603:234428, 2024.

[36] Seyed Saeed Madani, Erik Schaltz, and Søren Knudsen Kær. Effect of current rate and prior cycling on the coulombic efficiency of a lithium-ion battery. *Batteries*, 5(3):57, 2019.

[37] Hao Wang, Wen L. Soong, S Ali Pourmousavi, Xinan Zhang, Nesimi Ertugrul, and Bingyu Xiong. Thermal dynamics assessment of vanadium redox flow batteries and thermal management by active temperature control. *Journal of Power Sources*, 570:233027, 2023.

[38] Marnie Shaw, Bjorn Sturmberg, Lin Guo, Xinyu Gao, Elizabeth Ratnam, and Lachlan Blackhall. The NextGen energy storage trial in the ACT, Australia. In *Proceedings of the Tenth ACM International Conference on Future Energy Systems*, pages 439–442, 2019.

[39] Origin Energy. Electricity and natural gas offers, December 2023.

[40] Thomas Mercier, Mathieu Olivier, and Emmanuel De Jaeger. The value of electricity storage arbitrage on day-ahead markets across europe. *Energy Economics*, 123:106721, 2023.

[41] Binyu Xiong, Jinrui Tang, Yang Li, Changjun Xie, Zirui Wang, Xinan Zhang, and Hoay Beng Gooi. Design of a two-stage control strategy of vanadium redox flow battery energy storage systems for grid application. *IEEE Transactions on Sustainable Energy*, 13(4):2079–2091, 2022.

[42] Hao Wang, S Ali Pourmousavi, Wen L. Soong, Xinan Zhang, Nesimi Ertugrul, and Bingyu Xiong. Model-based nonlinear dynamic optimisation for the optimal flow rate of vanadium redox flow batteries. *Journal of Energy Storage*, 68:107741, 2023.